SOME HIGH PRESSURE STUDIES IN METALS AND ALLOYS

S. Ramaseshan
Materials Science Division
National Aeronautical Laboratory
Bangalore-17

ABSTRACT

A high pressure research group has been formed at Bangalore and this paper reports the work done by this group. It deals with (a) the experimental facilities set up, (b) the determination of the unified magnetic phase diagram of chromium and its dilute alloys, (c) the semiconductor to metal transition of rare-earth chalcogenides and (d) the studies on the electron collapse in liquid caesium.

1. INTRODUCTION

At the Materials Science Division of the National Aeronautical Laboratory we have a group working on the properties of materials at very high pressures. The project got impetus when we invited A. Jayaraman of the Bell Telephone Laboratories to spend some time with us. The actual work on the setting up of the 1000 ton press was commenced in March 1971 under his guidance and the entire fabrication was done in the workshops of our laboratory. Extensive facilities for high pressure X-ray research have also been built. A.Jayaraman left in September 1971 after erecting the press, initiating us into many problems and obtaining for us many materials for research.

In this paper I hope to mention briefly the equipment that have been constructed and review the investigations done in our laboratory, on problems relating to the metallic state. These are: (a) the determination of the unified magnetic phase diagram of chromium and its dilute alloys. (b) the study of the electronic transformation of rare-earth chalcogenides and (c) the theoretical

Lecture delivered at the Indian Institute of Metals , , 0

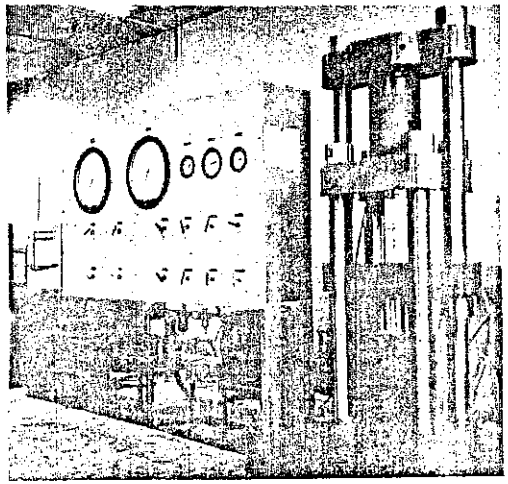

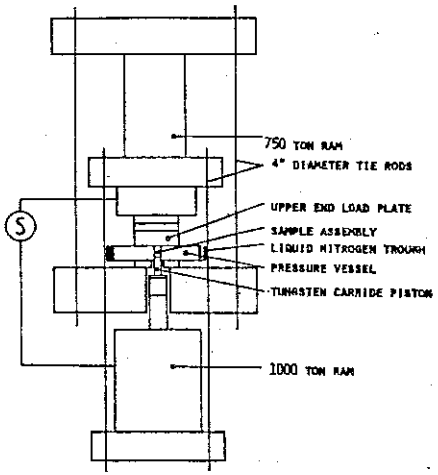

Fig.1 (top): The 1000 ton press at NAL.
Fig.2 Details of the parts. The maximum hydraulic pressure is 30,000 psi. The connecting stainless steel plumbing can withstand 60,000 psi. EN 24/4340 steel is used for the cylinders, rams, tie rods and platens. The piston and cylinder of the pressure chamber are made of tungsten carbide.

interpretation of the strange behaviour of liquid caesium under pressure. In each case before presenting our results I hope to give the experimental and theoretical position in these fascinating fields.

Besides A. Jayaraman many scientists of our laboratory have been actively engaged in these problems. Mention must be made of R.V. Ramani and N.Narayana Iyer (instrumentation), A.K. Singh and A. Chatterjee (X-ray studies on rare-earth chalcogenides), Rajaram Nityananda and A.S. Reshamwala (the magnetic phases of Cr and its alloys) and T.G. Ramesh (properties of liquid caesium). In the preparation of this paper each one of them has contributed a great deal. They have also kindly permitted me to refer to many of their unpublished results.

2. INSTRUMENTATION AND TECHNIQUES

(i) 1000 ton Press:

Very high pressures are generated by the advance of a 1 inch or $\frac{1}{2}$ inch diameter piston into a cylinder both made of tungsten carbide (WC). The piston assembly is advanced by a 1000 ton master-ram. Since tungsten carbide is strong in compression (40 to 60 kbar) and weak in tension or shear, precautions have to be taken to see that the material is always under compression.

The WC core (with the cylindrical hole)is fitted into binding rings of hardened steel. It is also clamped axially by a 750 ton end-load ram. The purpose of the binding rings and the end load is to provide support for the core. If the core is not inside the binding ring, when the high pressure is generated within the cylinder a compressive radial stress and a tensile hoop stress are created which cause a shear along which the carbide may fail. With the binding ring both become compressive so that the shear in the xy plane perpendicular to the ram

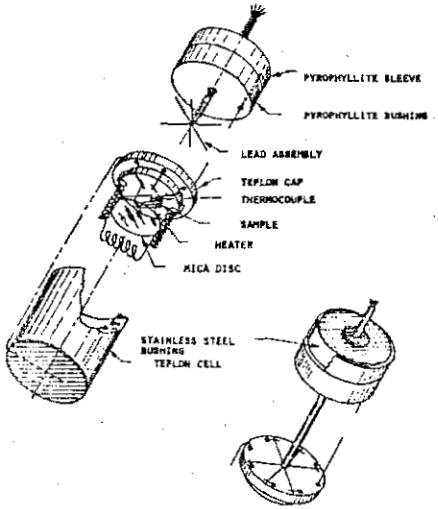

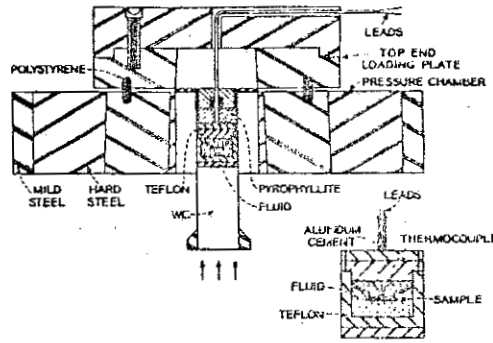

Fig.3 (left): Details of the teflon cell. The arrangement for 4 probe resistivity measurement (ref.2 and 3)

Fig.4 (right): The teflon cell positioned in the pressure chamber giving details of the binding ring, WC piston and cylinder.

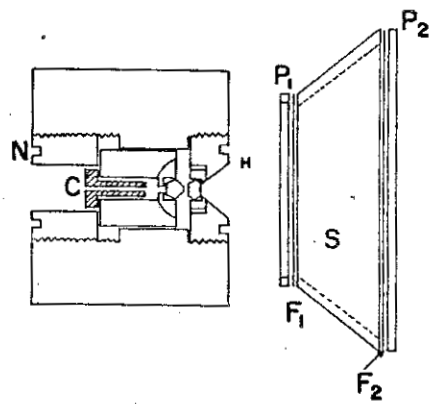

Fig.5 (a) Diamond anvil camera for pressures upto 300 kbar with the two film method for precision lattice parameters

Fig.5 (b) Typical photograph. Note reflexions from diamond.

movement z is minimised. However if there is no stress along the z axis there would again be a shear in the vertical plane which the end load ram counteracts by providing a compressive stress. It must be noted that the binding rings and the end load ram by providing static compressive load in all directions permit the use of the material with which the pressure chamber is made (WC) much beyond its normal operational capability. It is interesting that both the principles of the binding ring and end loading are to be found in Bridgeman's work[1]. Fig.1 shows the press and the control panel that were fabricated in our laboratory and Fig.2 is a line diagram detailing the different parts of the press.

(ii) Teflon cell technique for hydrostatic pressures:

Before 1967 one could attain hydrostatic pressures upto 30 kbar in the experimental chamber. The main difficulties in making measurements under hydrostatic conditions are the sealing of the liquid pressure medium and the introduction of electrical leads into the pressure chamber. A. Jayaraman et al[2] made an important advance when they developed the "teflon cell" technique which extended the range of hydrostatic pressure studies to 50 kbar. This enabled their group to study many new solid state phenomena at high hydrostatic pressures. A specially designed teflon cell (Fig.3) containing a liquid pressure medium is placed in the high pressure chamber where it is compressed by the advancing piston. Fig.4 shows the assembled cell in the pressure chamber. The electrical connections are drawn out through the cap of the cell and under pressure the system seals itself by the flow of teflon. The leads in the ceramic tube are gripped by pyrophyllite and stainless steel discs and this prevents their extrusion. 6 leads are taken out from the experimental chamber which makes four probe resistivity measurements and temperatures recording

simultaneously possible. Originally the cell was externally heated by passing a large A.C.current through a graphite sleeve. R.G. Maines[3] introduced the internal heating system (See Fig.3) which has the advantage of eliminating interference from the A.C. in the measuring circuits and extending the temperature range to 350°C.

All the measurements made at Bangalore at hydrostatic pressures use the teflon cell technique. The liquid pressure media are iso amyl alcohol (-50°C to 150°C), n pentane (-120°C to 120°C) and silicone oil (upto 350°C). Low temperatures down to -120°C are attained by pouring liquid nitrogen over the pressure plate (Fig.4).

(iii) High pressure X-ray diffraction instrumentation:

High pressure X-ray cameras are the most convenient instruments for studying structural changes as well as the pressure-volume relation upto 300 kbar[4,5]. Structural changes occurring at high pressures can easily be detected by the appearance of new sets of lines in the diffraction pattern. Since most high pressure cameras give Debye-Scherrer powder patterns, simple structures can easily be identified. The determination of complex phases is made more difficult because the accuracy in the d-spacings determined in high pressure cameras is poor. This is because MoK radiation is invariably used to minimise absorption by the pressure vessel so that only low angle reflexions are recorded. In spite of these difficulties extremely interesting results on pressure induced phase transitions and in pressure-volume relations have been obtained. Recently single crystal high pressure X-ray cameras[6] have been developed but the pressure range is limited to 30 kbar.

(a) Diamond anvil cameras: The hardness and the strength of diamond as also its low X-ray absorption, make

it the best substance for making high pressure X-ray cameras[7,8]. We have constructed a diamond anvil camera based on the design of Bassett et al[9]. The basic features are schematically shown in Fig.5. The sample is placed between two diamond faces and pressure is applied by tightening the nut N. The collimator C permits a narrow beam (100μ or 50μ) to pass through the diamond anvils and the specimen. The diffracted beam ($2\theta < 45^{\circ}$) escapes through a small slit in the diamond holder H and strikes the photographic film. The stationary diamond face is 2 mm in diameter while that on the collimator side is smaller and about 0.3 to 0.5 mm across. With this we have been able to reach pressures upto 300 kbar. The pressure attainable and the life of the diamond anvils depend very much on the parallelism of the two faces which for optimum performance have to be aligned optically[9].

(b) Tungsten carbide anvil cameras: Unlike in a diamond camera the X-ray beam has to pass perpendicular to the pressure axis in a tungsten carbide anvil camera because of the high absorption of WC to X-rays. Based on the designs of McWhan and Bond[10] and of Lawson and Jamieson[11] we have constructed (Fig.6) a tungsten carbide anvil camera[12]. The sample is inserted in a small hole (7 mils) drilled in a small boron-epoxy (3:1) disc. The boron disc is placed between two tungsten carbide pistons and the pressure is applied with a 5-ton hydraulic ram. The specially designed film cassette is shown in Fig.6b. The quality of the diffraction pattern is in general poor due to the background produced by the scattering from the boron disc. The use of filtered or crystal monochromated radiation improves the background but increases the exposure time considerably.

(c) Precision lattice parameter measurement: A cylindrical or a flat film cassette is normally used with the high pressure cameras. However, the uncertainty

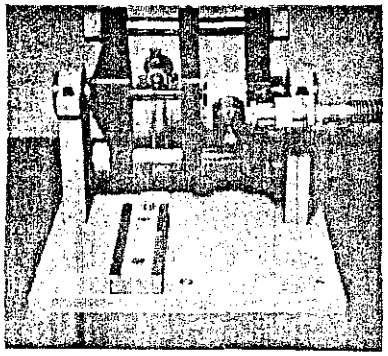

Fig.6(a) left:: Tungsten carbide anvil camera. The 5-ton hydraulic ram, the tie rods, the WC pistons, collimator and the track for the cassette are seen.

Fig.6(b) right: The special sector cassette which can be slided in and removed without disturbing the press etc.

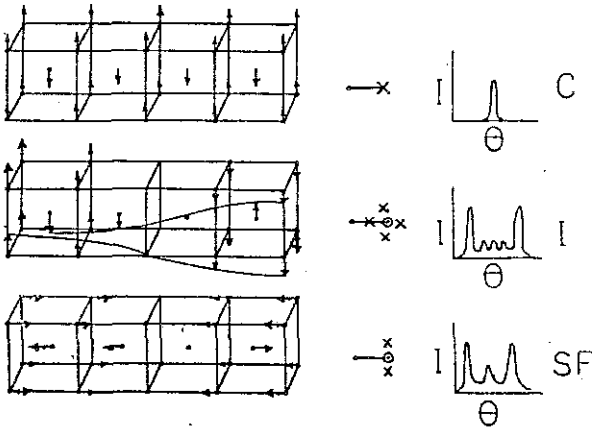

Fig.7 (a) The commensurate (C), incommensurate (I) and spin flip (SF) antiferromagnetic structures for a bcc lattice.

(b) One nuclear reciprocal lattice point and the associated points of magnetic origin shown in projection for the C, I and SF

(c) The neutron diffraction peaks of magnetic origin observed in a single(multidomain)crystal rotation pattern for C, I and SF.

in the sample-to-film distance and the absorption of the radiation in the sample introduce errors in the d-spacings. These errors are appreciable since only low angle lines are recorded in these cameras. These errors can be eliminated by recording the diffraction patterns, first on flat film and then giving a second exposure after displacing the film through an accurately known distance X. The diffraction angle 2θ can be calculated from a simple relation

$$\tan 2\theta = \frac{d_1 - d_2}{2(X_1 - X_2)} = \frac{d_1 - d_2}{2X}$$

where d_1 and d_2 are the ring diameters of a particular line for sample-to-film distances X_1 and X_2 respectively. In view of long exposures required in high pressure cameras this is not very practicable. A film cassette has been constructed[13] which permits the simultaneous recording of the X-ray diffraction patterns on two flat films separated by an accurately known distance X. The principle is shown in Fig.5. Two films are placed in tandem. Since MoK radiation is not absorbed much by X-ray films, two good patterns are recorded simultaneously on the films F_1 and F_2. A typical pattern obtained with the two-film cassette is shown in Fig.5b. This arrangement is now routinely used in our investigations and the higher accuracy is expected to be valuable in the p-v relation as also in identifying complex structures.

(d) Pressure estimation: The pressure on the sample is commonly estimated by mixing with the sample some substance of known compressibility. Obviously the pressure marker should give a simple diffraction pattern and should have high compressibility and the pressure volume relation should be known accurately. NaCl is commonly used

as a pressure marker. It has a high compressibility and its p-v relation is known accurately[14]. Other substances such as silver are commonly used in high pressure ranges ($\approx$ 100 kbar) in diamond anvil cameras. The accuracy of volume obtained is 0.6 percent while that of pressure is only 5 percent.

3. MAGNETIC PHASES OF CHROMIUM AND ITS ALLOYS

Some rather novel methods of establishing the phase diagrams of the antiferromagnetic phases of chromium and its alloys have been undertaken in our laboratory. Before reporting these it seems relevant to review very briefly the present state of knowledge in this field.

(i) Magnetic properties of pure chromium[15,16].

Pure Cr is antiferromagnetic at room temperature and its Neel temperature T_N at atmospheric pressure is 311°K.above which it is paramagnetic (P). The magnetic structure is incommensurate antiferromagnetic. Fig. 7a shows the case when a bcc lattice ~~which~~ is commensurate antiferromagnetic (C), where all the atoms at the cube vertices have identical up magnetic moments, while those at the body centres have equal down moments. Magnetic neutron diffraction studies give typical values of 0.5 Bohr magneton per atom along the (100) and the equivalent cubic directions. Pure Cr does not exhibit the commensurate phase. This phase occurs, however, in many of the alloys of chromium[17]. The incommensurate phase (I) of chromium differs from the commensurate (C) in that the moments in both the sub-lattices are modulated with a periodicity of n lattice spacings where n need not be integral. Further n is a function of temperature. Fig.7a illustrates a case where n=8 whereas in chromium n is close to 20. Below 120°K in pure Cr at atmospheric pressure the polarisation changes from transverse to

longitudinal and this is called the spin flip (SF) transition.

These phases may be described in terms of the reciprocal lattice through which one may visualise the neutron diffraction patterns. The nuclear reflexions and the magnetic reflexions of the commensurate phase form two separate fcc lattices. When both the nuclear and magnetic reflexions are considered the reciprocal lattice is simple cubic. For the incommensurate phase one also has a reciprocal lattice vector of $2\pi/na$ so that a large number of magnetic reflexions can, in theory, occur between the nuclear reflexions. In practice however, the magnetic reflexions occur only at $(2\pi/a)(1 \pm 1/n)$ which would correspond to the splitting of the magnetic reflexion of the commensurate phase into two. The crystal, in reality, consists of three types of domains with the sinusoidal modulation along the (100), (010) and (001) directions. Fig.7b presents projections in reciprocal space of a single nuclear reflexion and the associated magnetic reflexions. Fig.7c gives the magnetic reflexions (observed with a multidomain crystal) associated with one nuclear reflexion. The commensurate phase (C) gives one magnetic reflexion while I gives five and SF three.

(ii) Magnetic properties of Cr alloys[17]:

If pure Cr is alloyed with elements like V, Nb or Ta with electron to atom ratio (e/a) less than 6 the Neel temperature T_N is depressed and the magnetic moment μ decreases. When (e/a) = 6 for the additives (Mo, W) T_N and μ behave in a similar manner. In both the cases it is found that $\mu_{alloy}/\mu_{Cr} = (T_N)_{alloy} / (T_N)_{Cr}$. The addition of elements with e/a > 6 (viz. Mn, Ru, Re, Tc) raises T_N. When the nett (e/a) of the alloy is less than 6.005 one observes the incommensurate phase I

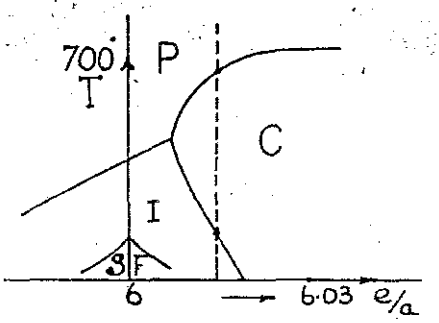

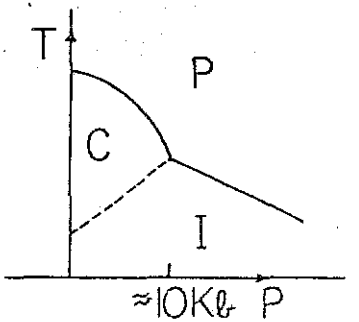

Fig.8 (left): A schematic phase diagram showing the observed magnetic phases of Cr alloys as temperature (T) and electron to atom ratio (e/a) are varied.

Fig.11 (right): The effect of pressure on T_N and T_{IC} for an alloy with e/a = 6.01 (Schematic)

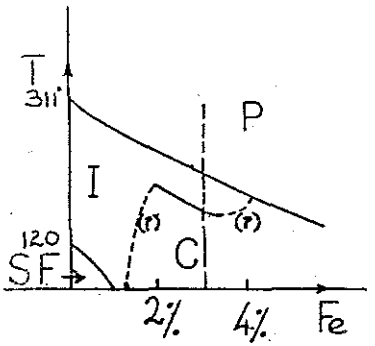

Fig.9. A phase diagram showing the observed magnetic structures of Cr-Fe alloys as temperature (T) and the percentage of Fe are varied. Schematic after Ishikwa et al (ref.18)

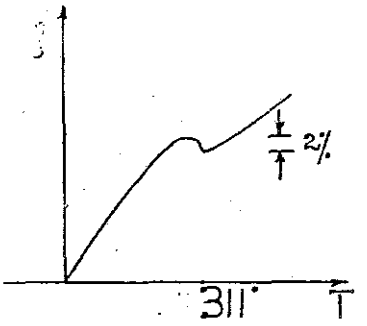

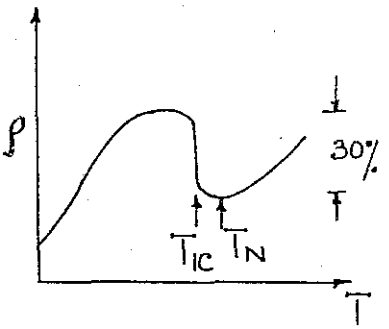

Fig.10 (left): The resistivity of pure Cr as a function of temperature (Schematic)

Fig.12 (right): The resistivity of Cr 3 percent Fe as a function of temperature (Schematic)

as in pure Cr (Fig.8). For a slightly higher concentration T_N shoots up and the commensurate phase appears at higher temperatures. This is illustrated schematically in Fig.8. The ordering sequence when an alloy of (e/a) = 6.01 is cooled (dotted line in Fig.8) would be P-C-I. When (e/a) increases to 6.02 (say) the field of the C phase widens and the I phase disappears.

(iii) Magnetic properties of Cr-Fe alloys[18,19]:

These alloys behave in a manner very different from the Cr-Ru alloys although both Fe and Ru have (e/a) = 8. For Fe less than 2 per cent T_N decreases whereas the magnetic moment increases. The alloys are incommensurate in the whole temperature range. When the iron content is between 2 percent and 3 percent, T_N continues to decrease and on cooling (dotted line) the order of phases is P-I-C in contrast to P - C - I in Cr-Ru alloys. When the iron content is greater than 5 percent the P - C transition is only seen. All these effects are schematically shown in Fig.9.

(iv) Transport properties and the pressure effects on Cr and its alloys:[20]

At the Neel temperature pure Cr exhibits a resistivity anomaly as shown schematically in Fig.10 and the anomaly is approximately 1 to 2 percent. Since resistivity can be measured under high pressure, it can be used as a probe to follow T_N as a function of pressure. It is found that T_N decreases with pressure and under certain circumstances, the antiferromagnetism is even suppressed completely[21]. In an alloy like Cr 1 percent Mn or Cr 0.6% Ru at atmospheric pressure two transitions P - C and C - I have been observed by neutron diffraction (Fig.11). Resistivity measurement reveal only the P - C transition.

Unfortunately the I - C transition does not exhibit itself as a resistivity change. In these alloys T_N first falls rapidly with pressure. At a particular value of P there is a sudden break in the slope dT_N/dP after which the rate of fall of T_N is very much slower (Fig.11). This slope corresponds to that seen in pure Cr. In fact it is found that the slope dT_N/dP can be used as an effective criterion to decide whether a P - C or a P - I transition is being observed, the latter having a very much smaller slope.

Reverting back to Fig.11, if one interprets the break in the slope as a triple point then there are two known points on the I - C line, the other being the one at P=0 obtained from neutron scattering. The line joining these two points gives an approximate phase boundary. The slope of this line is confirmed by thermal expansion experiments at higher pressures[22]. The basic phase diagram shown schematically in Fig.11 is well substantiated even though neutron scattering experiments under pressure have not been done. It is most interesting to compare the T vs P phase diagram (Fig.11) with that of T against e/a (Fig.8) obtained from neutron scattering. One sees that these two diagrams are roughly mirror images of each other. There appears to be an empirical correspondence between e/a increase and pressure decrease or vice versa. An addition of 1 percent Mn or $\frac{1}{2}$ percent Ru to Cr increases the (e/a) ratio by 0.01 and the effect of this can be off-set by approximately 6 kbar pressure.

(v) Resistivity of Cr-Fe alloys[22]:

Again Cr-Fe alloys behave very differently from the other alloys. The typical schematic curve of ρ vs T is shown in Fig.12 and this may be compared with the curve for the other Cr alloys (Fig.10). The following are the

salient features of the resistivity curve for Cr 3 percent Fe: (a) It shows a minimum corresponding the value of T_N as obtained from neutrons scattering. (b) On further cooling a sharp rise in the resistivity is observed and this temperature agrees with T_{IC}. (c) both T_N and T_{IC} fall with pressure (Fig.13) and (d) the sharp anomaly disappears above 2.5 kbar. The phase diagram is shown schematically in Fig.13.

(vi) General unified phase diagram of Cr and the effect of alloying with iron[23]:

From the brief review many questions may be raised concerning the Cr-Fe alloys. (a) Why is the ordering sequence on cooling P - I - C and not P - C - I as in Cr-Ru alloys? (b) Why do not the Cr-Fe alloys exhibit a triple point between P, C and I?

Rajaram Nityananda, A.S. Reshamwala and A. Jayaraman[23] found from extrapolating the boundaries of Cr 3% Fe (Fig.13) that there is a triple point at about -2 kbar. They deduced that the addition of ½ percent Ru or 1 percent Mn would be equivalent to a negative pressure and would make this triple point observable. Pressure experiments on Cr 3% Fe 0.5%Ru and Cr 3 % Fe 1% Mn strikingly confirmed their expectation.

The resistivity curves at various pressures for the first alloy are shown in Fig.14. It can be seen from the atmospheric pressure curve that the resistive anomaly has been considerably rounded off and the Neel temperature raised by 100^0 from the value for Cr 3 percent Fe. Application of pressure lowers T_N and the slope suggests that we are seeing the P - C transition.

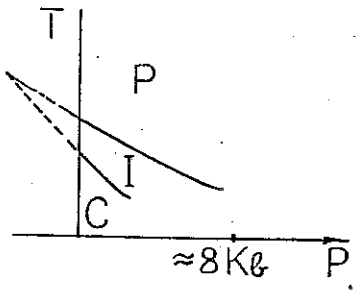

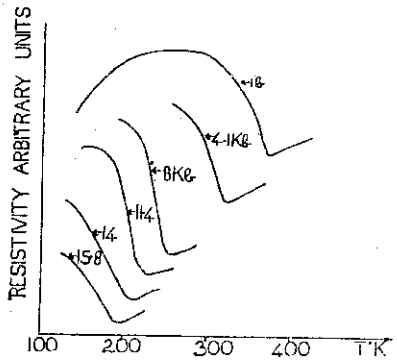

Fig.13 (left): The effect of pressure on T_N and T_{IC} for Cr 3 percent Fe (Schematic)

Fig.14 (right): The resistivity temperature curves for Cr 3 percent Fe ½ percent Ru at various pressures (Rajaram Nityananda et al[23])

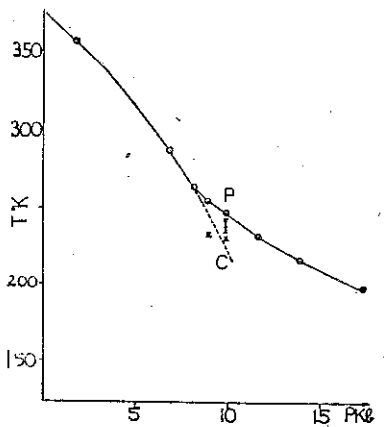

Fig.15: The effect of pressure on T_N and T_{IC} for Cr 3 percent Fe ½ percent Ru (ref.23)

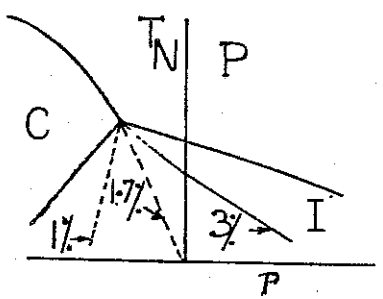

Fig.16: The unified phase diagram for Cr alloys showing the effect of Fe addition on the I - C boundary

Between 8 and 12 kbar pressure the resistive anomaly is very steep, this being perhaps the first Cr alloy to exhibit a sharpening of the resistive anomaly under pressure. At 8 kbar there is break in the slope of the T_N-P curve indicating a triple point. The reduced slope above this pressure corresponds to a P - I transition. Further the location of the steep rise in resistivity gives the temperature of the I - C transition. Above 12 kbar the resistive anomaly again rounds off. The results derived from these experiments are plotted as a phase diagram in Fig.15.

The authors could unify the behaviour of Cr-Fe alloys with that of the other alloys on a single phase diagram which is shown schematically in Fig.16.

The full lines represent the phase diagram of pure chromium. In the positive pressure region one observes only the P and I phases. The effect of V, Nb, Ta ($e/a < 6$) can be represented by displacing the zero pressure axis to the right (lowering T_N). The effect of alloying with element Ru, Mn, Re, Tc ($e/a > 6$) can be represented by displacing the zero pressure axis to the left. This raises T_N and introduces the commensurate phase at higher temperatures making the triple point observable.

On this phase diagram we represent the effect of the addition of iron as a rotation of the I - C boundary. Below a critical concentration of iron we would still observe only the P and I phases. For Cr 3 percent Fe alloy the phase boundary would have reached the position shown in the positive pressure region accounting for the P - I - C sequence.

This work has many interesting implications with regard to the transport properties and the entropy of the

I and C phases as influenced by the local moment known to exist on the iron atom[23]. But these questions will not be dealt with here.

4. RARE EARTH CHALCOGENIDES - HIGH PRESSURE X-RAY STUDIES

Rare-earth chalcogenides are metallic or semiconducting depending on whether the rare earth ion is in the trivalent or the divalent state[24]. Most semiconducting rare earth chalcogenides exhibit pressure induced semiconductor-metal transition. SmSe and SmTe[25] which crystallise, as most rare-earth chalcogenides do, in the NaCl structure, undergo a continuous semiconductor-metal transition in the 1 - 30 kbar-range while SmS[26] becomes conducting at 6.5 kbar. These transitions are due to the promotion of the 4f electrons to the 5d state which results in the conversion of the divalent ion to the trivalent state. Such a change should obviously be accompanied by a large volume change. We have undertaken the investigation of the pressure-volume relation of some rare-earth chalcogenides near the semiconductor-metal transition.

The pressure volume relations[27] for SmTe are shown in Fig.17. The pressure volume curve for SmTe is anomalous in the range 20 to 60 kbar. The measurement of resistivity as a function of pressure indicates that in this pressure range the resistivity drops by four orders of magnitude. The anomalously large volume change in this pressure range is due to the continuous conversion of Sm^{++} to Sm^{+++}. The large discontinuity near 100 kbar is due to the structural transformation from NaCl to CsCl phase.

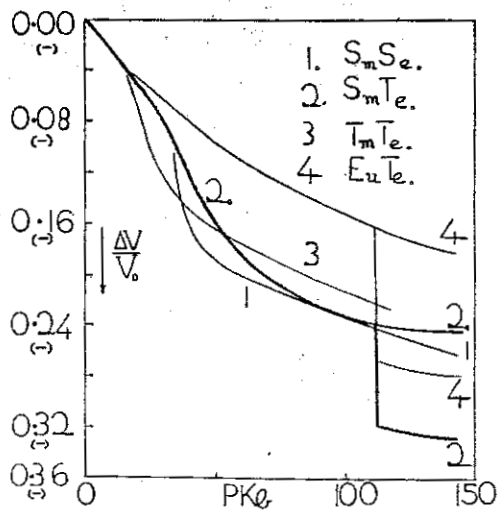

Fig.17: Pressure-volume relation for some rare-earth chalcogenides. EuTe shows a normal p-v curve. Anomalously large volume changes in the case of SmSe, SmTe and TmTe are due to electronic transition involving 4f-5d electron promotion A.K. Singh et al (ref. 27, 28, 29, 30)

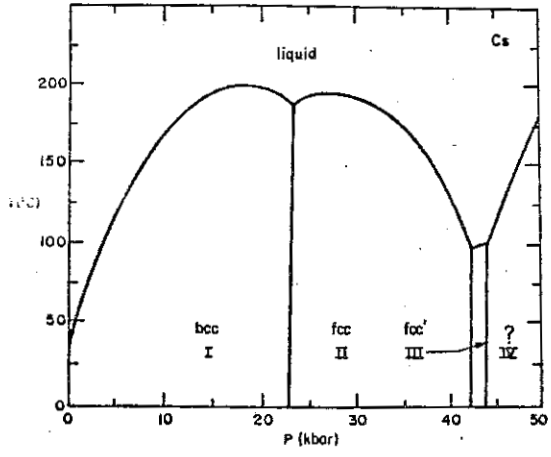

Fig.18: Fusion curve of caesium (Jayaraman et al. ref.34)

SmSe, SmS, TmTe, EuTe, YbTe have all been examined[28,29,30]. All except EuTe exhibit anomalous volume changes. EuTe shows no indication of any appreciable Eu^{++} Eu^{+++} conversion upto 150 kbar.

The nature of the pressure-volume curve can be explained by introducing a pressure dependent 4f-5d energy gap E(P). It can easily be shown that the volume change associated with RE^{++} RE^{+++} conversion is given by

$$\left(\Delta V/V_o\right)_{el} = (1 + \Delta a/ao)^3 - 1 \qquad ..(1)$$

where $\Delta a = 2(r^{+++} - r^{++}) \exp -(Eo - \alpha P)/ kT$ where r^{+++} and r^{++} are the ionic radii of the trivalent and divalent rare earth ions, a_o is the lattice parameter at atmospheric pressure, α is the rate at which the energy gap closes with pressure and Eo is the energy gap at atmospheric pressure. The value of Eo and α are available in a few cases from optical studies[31,32]. The actual pressure volume curve can be obtained by adding the normal compressibility term to eqn(1). The p-v curve thus obtained is in fair agreement with experiment.

5. TRANSPORT PROPERTIES OF LIQUID CAESIUM METAL

Before presenting the work done at Bangalore on the two species model of liquid caesium and the increase of its resistivity with pressure due to resonant scattering we shall briefly review the experimental and theoretical position in regard to this substance.

(i) The phase diagram of Caesium[33,34]:

The melting curve of Cs (i.e. the melting temperature T_M with pressure P) is given in Fig.18 . At 23 kbar the bcc structure transforms to the fcc structure. At 42.5 kbar there is a second transition exhibiting a

substantial decrease in volume although the structure continues to be fcc. This is attributed to a phenomenon called "electron collapse". The original suggestion that such a collapse could take place is due to Fermi[35]. In caesium the narrow and empty 5d band is above the Fermi level. With increase in pressure while the Fermi level is raised, the 5d band is lowered due to orbital overlap. At 42.5 kbar all the 6s electrons in the conduction band are scattered into the 5d band. Since 5d electrons are more localised, there is a shrinkage in the atomic volume. Cerium is probably the only other example in which electron collapse takes place[36].

The negative slopes following the two maxima in the fusion curve imply that the density of the liquid is higher than that of the solid phase below. This is a direct consequence of the Clausius-Clayperon equation ($dT/dP = \Delta V/\Delta S$). The increase in density immediately after the first maximum may be explained as due to the packing of atoms in the liquid being closer than the loosely packed bcc coordination in the solid. This argument fails to explain the increase in density in the region after the second maximum as the solid phase below is in the closest packed configuration. A simple assumption may be made that electron collapse takes place when the inter atomic distance equals that in the collapsed fcc phase in the solid. If this is taken as the empirical criterion, it is obvious that in the liquid, even at very much lower pressures, such a critical distance would be favoured over short ranges encompassing the first co-ordination shell. Thus in liquid Cs electron collapse could take place in these micro-regions. With increase of pressure the number of these micro-regions would increase, raising the concentration of the collapsed species.

(ii) Resistivity variation of liquid caesium[34]:

Since the transport properties are expected to be sensitive to electron collapse, Jayaraman and his co-workers[34] measured the resistivity of liquid Cs as a function of pressure. The experimental curve is shown in Fig.19. Qualitatively these experimental results lend support to the two species model[37]. However there are many features of the curve that require detailed explanation. These are (a) the shallow resistivity minimum at low pressures, (b) the rapid increase in resistivity by a factor of 4 in the 20 - 40 kbar region and (c) the flattening of the curve at higher pressures.

The investigations at Bangalore were undertaken to understand the mechanism of the electron collapse in the liquid state and to explain the main features of the ρ versus P curve.

(iii) Virtual bound state and electron collapse[38]:

If the two species model of liquid Cs presented earlier is basically correct one must enquire whether the lifetime of the collapsed atom is long enough to affect the physical properties. We give an atomic view of the electron collapse in the liquid state. Fig.20 presents the potential energy diagram schematically for both the 6s and the 5d electrons. An electron possessing the 6s character is acted upon by the attractive coulomb potential V_b/b of the caesium ion. On the other hand, as the 5d electron possesses an angular momentum ($l = 2$) it is also acted upon by a centrifugal potential term $l(l+1)/r^2$ which is repulsive in character and opposes the coulomb interaction. (The centrifugal term does not exist for the spherically symmetric 6s state as $l = 0$). Thus, the electron in the 5d state can be considered to be acted upon by an effective potential

$V_{eff} = V_b + \ell(\ell+1)/r^2$. The important feature of the V_{eff} vs. r diagram (Fig.20) is the creation of a barrier of finite height at a positive energy. In this figure, the energy state of the electron is also shown. The 6s to 5d electron collapse corresponds to the tunneling of the particle into the potential well as viewed from the side corresponding to higher values of r. This results in the formation of a virtual bound state which ensures a large life-time for the electron in the potential well. Since the electron corresponds to one of positive energy, it will eventually tunnel out of this region. Thus there would be a dynamic conversion between the normal and the collapsed species.

(iv) Resonance scattering and resistivity[38]:

A liquid metal unlike a crystalline one has only short range order. The scattering of electrons near the Fermi level by the liquid structure gives rise to the resistivity. This process is very much akin to the diffraction of X-rays or neutrons by a liquid. The Ziman formula for the resistivity of a liquid metal is given by

$$\rho = \frac{12\pi\Omega}{e^2\hbar v_F^2}\int_0^1 S(x)\{V(x)\}^2 x^3\,dx$$

where S(x) represents the structure factor, V(x) , the form factor or the scattering factor and $x = \sin\theta$, where 2θ is the scattering angle. This formula is for a one component system.

Since the resistance is due to the loss of momentum of the electron in the forward direction it is clear that scattering through large angles (close to π) would contribute most to the resistivity. The presence of the

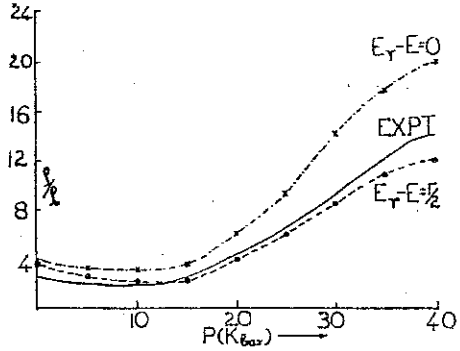

Fig.19: Resistivity vs. pressure diagram of liquid caesium. Experimental curve Jayaraman et al[34]. Theoretical Ramesh and Ramaseshan[38]

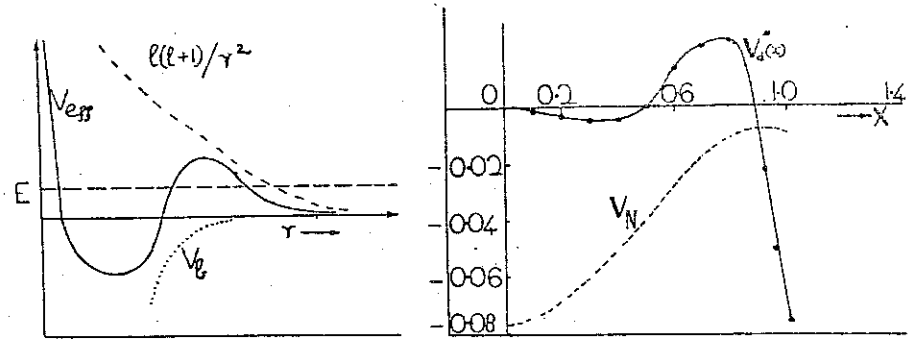

Fig.20 (left): Potential energy diagram for the 6s and 5d states and the formation of the virtual bound state.

Fig.21 (right): Form factors $V_N(x)$ and $V_d''(x)$ for Cs (ref. 38)

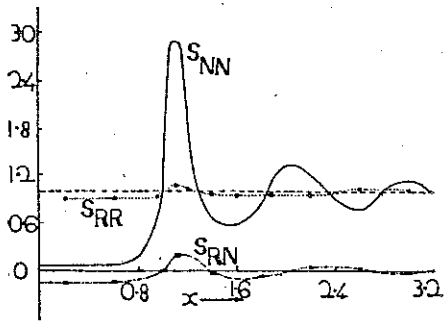

Fig.22: Partial Structure factors of a binary system of normal and collapsed atoms of Cs (ref.38)

factor x^3 in the integrand is an expression of this physical idea.

The structure factor S(x) describes the distribution of the diffracted intensity as a function of the scattering angle. This can be obtained by scattering experiments with X-rays or neutrons. One could also obtain it theoretically from a knowledge of the hard-sphere diameter and the packing fraction. This is dependent on the assumption that the short range order in a liquid is determined mainly from geometrical packing considerations[39]. The scattering factor V(x) can be evaluated by various methods like the model potential or the pseudopotential method[40]. The basic principle underlying these methods is that the strong potential of the ion can be replaced by a weak potential possessing the same scattering properties as that of the original potential. The screened form factor associated with this weak potential is shown in Fig.21.

In the case of liquid Cs we have to consider two species of atoms (in the normal and the collapsed states) with different hard-core diameters. The structure factor would therefore have to be modified to correspond to a binary liquid[41]. The more complicated aspect of the problem is to compute the difference in the form factors between the normal and the collapsed species. The latter are characterised by a large scattering factor which owes its origin to the long life-time of the electron in the virtual bound state. The scattering of electrons by the normal species can be described by a potential form factor $V_N(x) = V_o(x)$ while in the case of the collapsed species the d wave component of the scattering amplitude goes through resonance. The scattering factor for the collapsed species takes the form

$$V_R(x) = V_o(x) + V_d'(x) + i\, V_d''(x)$$

The notations are similar to those used in the anomalous scattering of X-rays or neutrons[42]. The resonant components V_d' and V_d'' can be calculated by the partial wave analysis method[43]. The variation $V_d''(x)$ with x is given in Fig.21. The important feature of this curve is the sudden dip in the region corresponding to back scattering on the Fermi surface, which would contribute considerably to resistivity. The formula for resistivity apprpriate to the two species system takes the form[44]

$$\rho = \frac{12\pi\Omega}{e^2\hbar\, v_F^2} \int_0^1 Z\, x^3\, dx$$

where $Z = C\, S_{RR}(x)\, V_R(x)\, V_R^*(x) + (1-C)\, S_{NN}(x)\, V_N^2(x)$

$$+ 2\sqrt{C(1-C)}\; S_{NR}(x)\, V_N(x) \left\{ V_o(x) + V_d'(x) \right\}$$

Here C is the concentration of the collapsed or resonant species (R). N is the subscript used for the normal species. $S_{NN}(x)$, $S_{NR}(x)$ and $S_{RR}(x)$ are the partial structure factors of the system. The partial structure factors were evaluated using the Percus-Yevick theory of binary liquid mixtures[41] and these are given in Fig.22. Using the form factors shown in Fig.21, and the concentrations calculated for a thermodynamic analysis[37] the resistivity can be evaluated.

(v) The variation of resistance with pressure in liquid Cs[38]:

In calculating the resistivity as a function of pressure, one has to consider the effect of the volume

contraction on (a) the radius k_F of the Fermi sphere (which is computed from the free electron formula), (b) the partial structure factors (which are obtained by changing the appropriate parameters in the Percus-Yevick expressions) and (c) the form factors (which are assumed not to be affected in our simplified model).

In the low pressure region, the concentration of the collapsed species is so small that, for most purposes the liquid can be considered to be a one component system. The magnitude of the isothermal compressibility decreases with increase of pressure so that the long wavelength limit of the structure factor $S_{NN}(0)$ decreases in accordance with the compressibility formula.[41] Thus the contribution to the resistivity integral from the low x region called the plasma resistance decreases with increase of pressure. On the other hand, the increase in the magnitude of k_F causes the upper limit of integration to sample regions of higher values of $S_{NN}(x)$ so that the contribution due to structural resistance increases. The shallow minimum in the resistivity is due to the slight preponderance of the former over the latter effect. As the pressure is further increased, the presence of the collapsed species cannot be ignored in view of their significant contribution to the resistivity integral. The steep variation in the 20-40 kbar region is due to the rapid increase in the concentration of the collapsed species. The tendency for saturation in the resistivity above 45 kbar can be understood if one assumes that the process of electron collapse is nearly complete. Fig.19 presents the experimental curve and the theoretically calculated curves for two values $E_d-E=0$ (corresponding to the case of exact resonance) and $E_d-E=\Gamma/2$ where Γ represents the width of the d-wave resonance. It can be seen that both these curves have

the same general features as that of the experimental curve giving support to the basic correctness of the theory.

REFERENCES

1. Bridgman, P.W., The Physics of High Pressure G.Bell and Sons, London (1949)

2. Jayaraman, A., Hutson, A.R., McFee, J.H., Coriell, A.S., and Maines, R.G., Rev. Sci. Inst. 38 (1967) 44.

3. Maines, R.G., Rev. Sci. Inst. 41 (1970) 1415.

4. Jamieson, J.C., and Lawson, A.W., Modern Very High Pressure Techniques, Ed. R.H. Wentorf, Butterworth (1962) 70.

5. McWhan, D.B., Trans. Amer. Cryst. Assoc. 5 (1969) 39.

6. Fourme, P.R., J. Appl. Cryst. 1, (1968) 23.

7. Davis, B.L., and Adams, L.H., J. Phys. Chem. Solids, 25 (1964) 379.

8. Piermarini, G.J., and Weir, C.E., J. Res. Natl. Bur.Stds (U.S.), 66A, (1962), 325.

9. Bassett, W.A., Takahashi, T., and Stook, W.P., Rev.Sci.Intr. 38, (1967), 37.

10. McWhan, D.B., and Bond, W.L., Rev. Sci. Intr. 35 (1964) 626.

11. Jamieson, J.C. and Lawson, A.W., J. Appl. Phys. 33, (1962), 776.

12. Singh, A.K., Chatterjee, A., and Narayana Iyer, N., N.A.L. Tech. Note.

13. Singh, A.K., Rev. Sci. Intr. (under publication).

14. Decker, D.L., J. Appl. Phys. 36, (1965), 157.

15. Bykor, V.N., Golovin, V.S., Ageev, N.V., Ledvik, V.A., and Vinogadrov, S.I., Dokl.Akad.Nauk.SSSR 128 (1959) 211.

16. Corliss, L., Hastings, J., and Weiss, R., Phys. Rev. Lett. 3 (1959) 211.

17. Koehler, W.C., Moon, R.M., Trego, A.L., and Mackintosh, A.R., Phys. Rev. 151 (1966) 405.

18. Ishikawa, Y., Hoshino, S., and Endoh, Y., J. Phys. Soc. Japan 22 (1967) 1221.

19. Arrott, A., Werner, S.A., and Kendrick, H., Phys. Rev. 153 (1967), 624.

20. Rice, T.M., Jayaraman, A., and McWhan, D.B., International Conference on Magnetism, Grenoble (1969).

21. McWhan, D.B., and Rice, T.M., Phys.Rev. Lett. 19 (1967) 846.

22. Syono, Y., and Ishikawa, Y., Phys.Rev. Lett. 19 (1967) 747.

23. Rajaram Nityananda, Reshamwala, A.S., and Jayaraman, A. (unpublished).

24. Iandelli, A., Rare Earth Research, Ed. E.V. Kleber, Macmillan, New York, (1961), 135.

25. Jayaraman, A., Narayanamurti, V., Bucher, E. and Maines, R.G., Phys.Rev. Lett. 25, (1970) 368.

26. Jayaraman, A., Narayanamurti, V., Bucher, E., and Maines, R.G. Phys. Rev. Lett. 25, (1970), 1430.

27. Singh, A.K., Jayaraman, A., and Chatterjee, A., Solid State Comm. 9, (1971), 1459.

28. Jayaraman, A., Singh, A.K., and Chatterjee, A., Ninth Rare Earth Research Conf. Virginia (1971).

29. Chatterjee, A., Singh, A.K., and Jayaraman, A., Phys.Rev. Lett. 27, (1971), 1571.

30. Singh, A.K., Chatterjee, A., Jayaraman, A., and Ramaseshan, S., Nucl.Phys. Solid State Phys. Symp. (BARC), S-105, (1972).

31. Wachter, P., Solid State Comm. 7, (1969) 693.

32. Francillon, M., Jerome, D., Achard, J.C., and Malfait, G., J.De.Phys. 31, 709, (1970).

33. Kennedy, G.C., Jayaraman, A., and Newton, R.C., Phys.Rev. 126 (1962) 1363.

34. Jayaraman, A., Newton, R.C., and McDonough, J.M., Phys. Rev. 159 (1967) 527.

35. Sternheimer, R., Phys. Rev. 78 (1950) 235.

36. Lawson, A.W., and Tang, T.Y., Phys. Rev. 76 (1949) 301.

37. Elizer Rapoport, J. Chem. Phys. 48 (1968), 1433.

38. Ramesh,T.G., and Ramaseshan, S, (to be published)

39. Wertheim, M.S., Phys. Rev. Lett. 10, (1963) 321

40. Harrison, W.A., Pseudopotentials in the theory of Metals, W.A. Benjamin, Inc., New York (1966).

41. Ashcroft, N.W., and Langreth, D.C., Phys.Rev. 156 (1967) 685.

42. Ramesh, T.G., and Ramaseshan, S., Acta Cryst. A27 (1971), 332.

43. Messiah, A., Quantum Mechanics, Wiley, New York (1965).

44. Ramesh, T.G., and Ramaseshan, S., J.Phys.C.(Solid State) 4, (1971).